Alternate formulation of enhanced backscattering as phase conjugation and diffraction: derivation and experimental observation

Jeremy D. Rogers,* Valentina Stoyneva, Vladimir Turzhitsky, Nikhil N. Mutyal, Prabhakar Pradhan, İlker R. Çapoğlu, and Vadim Backman

Northwestern University, 2145 Sheridan Road, Evanston, Illinois 60208, USA

**jdrogers@northwestern.edu*

Abstract: Enhanced backscattering (EBS), also known as weak localization of light, is derived using the Huygens–Fresnel principle and backscattering is generally shown to be the sum of an incoherent baseline and a phase conjugated portion of the incident wave that forms EBS. The phase conjugated portion is truncated by an effective aperture described by the probability function $P(s)$ of coherent path-pair separations. $P(s)$ is determined by the scattering properties of the medium and so characterization of EBS can be used for metrology of scattering materials. A three dimensional intensity peak is predicted in free space at a point conjugate to the source and is experimentally observed.

OCIS codes: (030.1670) Coherent optical effects; (290.1350) Backscattering; (050.1940) Diffraction.

References and links

1. A. Dogariu and G. D. Boreman, "Enhanced backscattering in a converging-beam configuration," Opt. Lett. **21**, 1718–1720 (1996).
2. N. C. Bruce, "A comparison of the converging and diverging geometries for measuring enhanced backscatter," J. Mod. Opt. **49**, 2167–2181 (2002).
3. P. Gross, M. Störzer, S. Fiebig, M. Clausen, G. Maret, and C. Aegerter, "A Precise method to determine the angular distribution of backscattered light to high angles," Rev. Sci. Instrum. **78**, 033105 (2007).
4. M. A. Noginov, S. U. Egarievwe, H. J. Caulfield, N. E. Noginova, M. Curley, P. Venkateswarlu, A. Williams, and J. Paitz, "Diffusion and pseudo-phase-conjugation effects in coherent backscattering from nd0.5la0.5al3(bo3)4 ceramic," Opt. Mater. **10**, 1–7 (1998).
5. F. Reil and J. E. Thomas, "Observation of phase conjugation of light arising from enhanced backscattering in a random medium," Phys. Rev. Lett. **95**, 143903 (2005).
6. Y. L. Kim, P. Pradhan, M. H. Kim, and V. Backman, "Circular polarization memory effect in low-coherence enhanced backscattering of light," Opt. Lett. **31**, 2744–2746 (2006).
7. E. Akkermans, P. Wolf, R. Maynard, and G. Maret, "Theoretical study of the coherent backscattering of light by disordered media," J. Phys. France **49**, 77–98 (1988).
8. P. Sheng, *Scattering and localization of classical waves in random media* (World Scientific Pub Co Inc, 1990).
9. M. I. Mishchenko, L. D. Travis, and A. A. Lacis, *Multiple Scattering of Light by Particles: Radiative Transfer and Coherent Backscattering* (Cambridge University Press, 2006).
10. E. Akkermans and G. Montambaux, *Mesoscopic Physics of Electrons and Photons* (Cambridge University Press, 2007).
11. R. T. Deck and H. J. Simon, "Simple diffractive theory of enhanced backscattering," J. Opt. Soc. Am. B **10**, 1000–1005 (1993).

#139056 - $15.00 USD Received 20 Dec 2010; revised 28 Apr 2011; accepted 27 May 2011; published 6 Jun 2011

12. T. Okamoto and T. Asakura, "Enhanced backscattering of partially coherent light," Opt. Lett. **21**, 369–371 (1996).
13. Y. Kim, Y. Liu, V. Turzhitsky, H. Roy, R. Wali, and V. Backman, "Coherent backscattering spectroscopy," Opt. Lett. **29**, 1906–1908 (2004).
14. J. Goodman, *Introduction to Fourier Optics* (McGraw-Hill Science, Engineering & Mathematics, 1996).
15. V. Turzhitsky, J. D. Rogers, N. N. Mutyal, H. K. Roy, and V. Backman, "Characterization of light transport in scattering media at subdiffusion length scales with low-coherence enhanced backscattering," IEEE J. Sel. Top. Quantum Electron. **16**, 619 –626 (2010).
16. M. Born and E. Wolf, *Principles of Optics*, 7th ed. (Cambridge University Press, 1999).

1. Introduction

Enhanced backscattering (EBS) or coherent backscattering refers to a peak observed in the angular profile of diffusely scattered light centered on the retro-reflection angle. The phenomenon is related to strong or Anderson localization that occurs in strongly disordered systems, but is observed in weakly scattering media where light is not completely confined but merely concentrated, and so it is also referred to as weak localization of light. EBS has been studied in a wide range of configurations. Previous reports on the observation of EBS in a converging or diverging beam configuration have demonstrated a corresponding broadening or narrowing of the peak [1, 2]. Detection of EBS along an arc in free space has been used to measure EBS at large angles covering up to a hemisphere [3]. Others have studied phase conjugation of the backscattered wave that forms the peak [4, 5]. Study of the polarization state preservation in Low-coherence Enhanced Backscattering Spectroscopy (LEBS) [6] can also be interpreted as phase conjugation of the wavefront, since phase conjugation of a wavefront preserves the handedness of the circular polarization state. Derivations of EBS are found in the literature using concepts from condensed matter physics [7–9]. A physical optics perspective has also been discussed in conjunction with a quantum mechanical description [10]. Some have described the effect using diffraction [11], and others have studied EBS under partial spatial coherence [12, 13].

It is often useful to describe a phenomenon from alternate perspectives using different conceptual starting points for the benefit of scientists with varying backgrounds. In this paper, we present a derivation based on the Huygens–Fresnel principle applied to the waves exiting from coherent path-pairs. We show that this description is analogous to phase conjugation of a portion of the incident wave and diffraction from a virtual aperture, a description which will be useful to the optics community and those with a background in imaging. This view is consistent with previous observations of phase conjugation, diverging and converging beam behavior, and the effect of partial spatial coherence on EBS. It predicts that a peak in intensity is formed in free space at a point conjugate to any source and with a shape dictated by diffraction. We present experimental observation of that peak, elegantly demonstrating weak localization in three dimensions and show that an image of an extended source is formed in free space without optics due to the EBS effect.

2. Concept and theory

In order to describe the EBS phenomenon using the Hugens–Fresnel principle, we must first describe the complex amplitude exiting the medium. Conceptually, a wave incident on a scattering medium is sampled at each scatterer and forms wavelets that can re-scatter many times, eventually with some component in the backward direction. Since light transport is reversible, the wave incident at the point of an exiting wavelet has a component that follows the same path in the reverse direction. These two counter-propagating waves form a time-reversed path-pair each with equal accumulated phase. This description can be used to represent any random medium that multiply scatters light including discrete or continuous media. In the case of discrete scatterers the paths are countable while in continuous media the paths are uncountable,

#139056 - $15.00 USD Received 20 Dec 2010; revised 28 Apr 2011; accepted 27 May 2011; published 6 Jun 2011

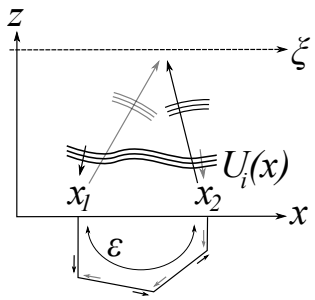

Fig. 1. Diagram illustrating the notation used in the derivation. The incident wave has complex amplitude $U_i(x)$ at the plane of the x-axis which represents the boundary or surface of the scattering medium. A time reversed path-pair begins and ends at points x_1 and x_2 with black arrows following counter-clockwise propagation and gray arrows following clockwise propagation. The phase ε of the common path is acquired by both counter-propagating waves. The exiting wavelets then propagate to the observation plane at distance z with coordinate ξ.

but in all cases (including finite or layered) the medium can be characterized by the distribution of paths as discussed later.

It should be noted that any path light follows as it scatters into the backward direction will have a time-reversed component associated with it. This path-pair can be represented by rays that connect the scattering points as light waves travel in each direction along the path. The first and last scatterers correspond to two exit positions of a path-pair, but there are generally many possible paths that share the same start and end point. The phase of each of these paths may be different, but upon exit, the sum of waves following these various paths results in a single effective phase and amplitude associated with that pair of exit points. We will hence refer to the sum of all paths sharing a common pair of exit points a path-pair. Since the counter-propagating waves exiting a path-pair have the same accumulated phase, the two exit points can be treated as a double pinhole and will result in classic diffraction patterns. However, the medium is made up of many path-pairs with varying orientation and separations, and consequently varying interference fringe spacing. For a single random ensemble, the result of interference of all possible path-pairs produces speckle. However, averaging over many ensembles of the medium (i.e. Brownian motion, spinning sample, etc.) requires treatment of the superposition of different path-pairs as incoherent. The sum of intensities is used, eliminating speckle and resulting in an intensity peak at the retro-reflection angle where the phase is equal for light that traverses each path-pair in opposite directions. The amplitude and phase of each independent path-pair is random, but with ensemble averaging, statistical parameters dominate.

2.1. Phase conjugation

Given the concept of time reversed path-pairs, one might expect that phase conjugation is involved. Assuming scalar waves, this can be shown by starting with an incident complex disturbance $U_i(x) = A_i(x)e^{i\phi_i(x)}$. If the path-pair samples this wavefront at two points x_1 and x_2, the phase exiting the medium will be given by the sum of the incident phase and the phase ε of the common path, $\phi_e(x_1) = \phi_i(x_2) + \varepsilon$ and $\phi_e(x_2) = \phi_i(x_1) + \varepsilon$. Likewise, the amplitude will be proportional to the incident amplitude at the opposite point and also a factor $\tilde{\alpha}$, that varies randomly for each path-pair. We factor out a constant $e^{i(\phi_i(x_1)+\phi_i(x_2)+\varepsilon)} = e^{ic}$ and use Dirac delta functions to represent the sampling operation.

#139056 - $15.00 USD Received 20 Dec 2010; revised 28 Apr 2011; accepted 27 May 2011; published 6 Jun 2011

$$
\begin{aligned}
A_e(x)e^{i\phi_e(x)} &= \tilde{\alpha}\delta(x-x_1)A_i(x_2)e^{i(\phi_i(x_2)+\varepsilon)} + \tilde{\alpha}\delta(x-x_2)A_i(x_1)e^{i(\phi_i(x_1)+\varepsilon)} \\
&= \tilde{\alpha}e^{ic}[\delta(x-x_1)+\delta(x-x_2)]A_i(x_1+x_2-x)e^{-i\phi_i(x)}
\end{aligned} \tag{1}
$$

If the incident amplitude is uniform, $A_i(x_1+x_2-x) = A_i(x)$ then the exiting complex amplitude for each path-pair is proportional to $U_i(x)^*$. This can be regarded as phase conjugation of a filtered or sampled portion of the wavefront.

2.2. *Diffraction from a virtual aperture*

Next, we apply the Huygens–Fresnel integral to propagate the complex amplitude to the plane of observation a distance z from the medium [14]. The complex amplitude for a single path-pair at point ξ in plane z is $U_z(\xi;x_1,x_2)$. Integration over x invokes the sifting property of $\delta(x)$ leaving the sum of two spherical waves centered at x_1 and x_2.

$$
U_z(\xi;x_1,x_2) = \frac{\tilde{\alpha}e^{ic}z}{i\lambda}\left[A_i(x_2)\frac{e^{ik\sqrt{z^2+(\xi-x_1)^2}-i\phi_i(x_1)}}{z^2+(\xi-x_1)^2} + A_i(x_1)\frac{e^{ik\sqrt{z^2+(\xi-x_2)^2}-i\phi_i(x_2)}}{z^2+(\xi-x_2)^2}\right] \tag{2}
$$

The contribution of all path-pairs can be calculated by integrating over x_1 and x_2, which results in a random signal since each path-pair has random phase and amplitude $\tilde{\alpha}e^{ic}$. Observation of EBS requires ensemble averaging, either by averaging independent observations or by integrating over time while the sample changes due to Brownian motion or rotation. If we assume that the phase of different path-pairs is uncorrelated, the ensemble average intensity is equal to the sum of the average intensity from each path-pair, $\iint \langle U_z(\xi;x_1,x_2)U_z^*(\xi;x_1,x_2)\rangle dx_1dx_2$, and the random phase e^{ic} cancels. The ensemble average of the remaining random parameter $\langle\tilde{\alpha}^2\rangle$ corresponds to the probability distribution $P(s)$ of path-pair separation, $s = |x_2-x_1|$. This distribution $P(s)$ is the defining characteristic of the random medium. In general, no analytical solution exists for P(s), but this distribution can be obtained using approximations (i.e. the diffusion approximation), or by numerical methods such as Monte Carlo simulation. We can also employ the Fresnel approximation when $z \gg \xi - x$ so the denominator in Eq. (2) becomes z^2 and radical in the exponent becomes $z+(\xi-x)^2/(2z)$. The entire operation of backscattering from a random medium is then written as Eq. (3).

$$
\begin{aligned}
\langle I_z(\xi)\rangle = \iint \frac{P(s)}{\lambda^2 z^2}\Big[&A_i^2(x_1)+A_i^2(x_2)+A_i(x_1)A_i(x_2) \\
&\times\left(e^{i\frac{k}{2z}((\xi-x_2)^2-(\xi-x_1)^2)+i\phi_i(x_1)-i\phi_i(x_2)} + e^{-i\frac{k}{2z}((\xi-x_2)^2-(\xi-x_1)^2)-i\phi_i(x_1)+i\phi_i(x_2)}\right)\Big]dx_1dx_2
\end{aligned} \tag{3}
$$

The assumptions made up to this point are the same as those made for Fresnel diffraction, namely: (1) scalar waves, (2) $z \gg \lambda$, and (3) $z \gg \xi - \{x_1 \text{ or } x_2\}$.

Some additional simplifications can be made if we assume illumination is uniform, $A_i(x_1) = A_i(x_2) = A_i$. We can use $A_i(x) = rect(x)$ to model a finite spot size, and for simplicity we assume the spot size is much broader than the function $P(s)$ so that $\iint A_i^2 P(s)dx_1dx_2 = aA_i^2$ where a is the area of the illumination. Next, we treat the special case of a diverging spherical wave from a point source on the z-plane at $\xi = 0$, the incident phase is given by $\phi_i = kx^2/(2z)$. Starting with Eq. (3), the x^2 terms of the exponent exactly cancel, and the equation can be written in cosine form.

$$
\langle I_z(\xi)\rangle = \frac{2aA_i^2}{\lambda^2 z^2}\left[1+\frac{1}{a}\iint_{A_i} P(s)\cos(\frac{k}{z}\xi(x_2-x_1))dx_1dx_2\right] \tag{4}
$$

Since $P(s)$ is symmetric, the inner integral over x_1 is a Fourier transform of $P(s)$ about each point x_2, and the outer integral is then the sum of these Fourier transforms from each x_2. If we

#139056 - $15.00 USD Received 20 Dec 2010; revised 28 Apr 2011; accepted 27 May 2011; published 6 Jun 2011

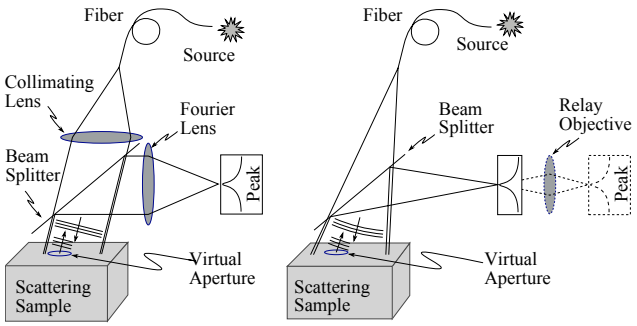

Fig. 2. Schematic of experimental setups for observation of EBS. Left: a typical configuration with a collimated beam and lens-detector system that measures angular intensity distribution. Right: our system comprised of simply a source, beam-splitter, and detector. Optionally, the peak is relayed to the detector using a microscope objective. In both cases, the reflected wavefront can be represented as a diffuse background plus a superposition of phase conjugated wavelets diffracted by the virtual aperture $P(s)$ to form the intensity peak at a point in space conjugate to the source.

again make use of the fact that the spot size is much larger than $P(s)$ and ignore the effect of the edge of the spot, the transform is independent of shift x_2 and the outer integral reduces to a factor of a.

$$\langle I_z(\xi)\rangle = \frac{2aA_i^2}{\lambda^2 z^2}\left[1+\int P(s)\cos(\frac{k}{z}\xi s)ds\right] \tag{5}$$

Ignoring edge effects, $\langle I_z\rangle$ is then proportional to $1+\mathscr{F}\{P(s)\}$. The Fourier transform can be thought of as representing diffraction by a virtual apodized aperture described by the function $P(s)$.

2.3. Partial spatial coherence and extended sources

The use of an extended source as the illumination has the effect of introducing a finite spatial coherence at the surface of the scattering medium. This can be treated in either of two ways. The coherence function can be said to further limit the virtual aperture [multiplication $P(s)\times C(s)$], or equivalently, each point in the extended source can be thought to produce an independent (incoherent) peak. The resulting peak is the convolution of the coherent peak with the source function as shown by applying the superposition integral. The van Cittert–Zernike theorem shows that when $C(0)=1$, these two conceptualizations are mathematically equivalent: $\langle I(\xi)\rangle \propto 1+\mathscr{F}\{P(s)\times C(s)\} = (1+\mathscr{F}\{P(s)\})*\mathscr{F}\{C(s)\}$.

3. Experimental observation

A typical experimental setup for observation of EBS uses a collimated laser beam to illuminate a random medium. The reflected light is focused by a lens that maps angles to positions on a detector. The peak is conventionally described in angle space relative to the incident beam. It could also be said that since the illumination is collimated, the source appears to be located infinitely far from the sample and the peak will be localized at infinity. The peak can instead be brought to focus on a detector by inserting a lens. An example of this geometry is shown on the left in Fig. 2.

The derivation in this paper shows that no lenses are necessary, and that a source located a finite distance from a random medium will produce an intensity peak in free space at any point conjugate to the source due to phase conjugation. This method of observing the phenomenon

#139056 - $15.00 USD Received 20 Dec 2010; revised 28 Apr 2011; accepted 27 May 2011; published 6 Jun 2011

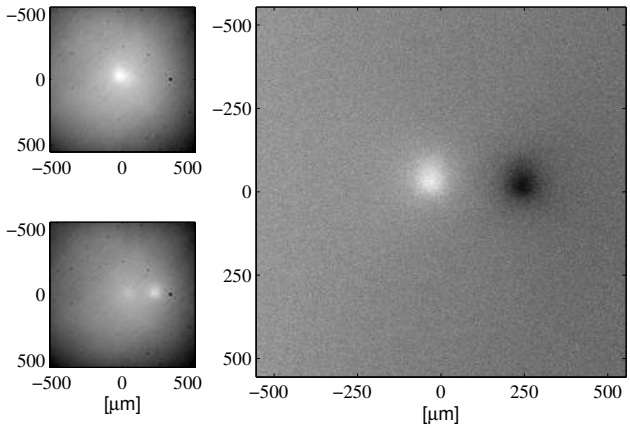

Fig. 3. The peak is measured for two different fiber positions. The first peak is normalized by the second resulting in a flat baseline, a true positive peak, and an inverted peak.

eliminates all lenses and elegantly demonstrates three dimensional weak localization of light. This 'lensless' geometry is shown in the diagram on the right of Fig. 2.

Our experimental geometry is extremely simple. The source is a step index multimode optical fiber with 50 μm diameter core and 0.22 Numerical Aperture (NA). Since the multi-mode fiber scrambles the phase and polarization, any type of illumination may be used. We have observed the peak using an arclamp, HeNe laser, or as with the experimental results shown here, a high-brightness LED with peak wavelength 635 nm and 20 nm bandwidth (FWHM). The fiber is tilted at an angle relative to the surface such that the no ray from the source is normally incident on the sample, ensuring that the specular reflection is separated from the peak. The diverging beam passes through the beam-splitter and illuminates the sample mounted on a stage to allow scanning in the z-direction. Backscattered light is reflected by the beam-splitter and the peak is formed at the point in space conjugate to the source.

Alignment of the detection plane is very simple since the peak is formed at the 3D location conjugate to the source. An experimentalist can place an eye to the left of the beam-splitter in Fig. 2 and observe the reflection of the source through the beam-splitter. The detector can be seen through the beam-splitter and can be aligned so that the source is centered and at the same depth as the detector. The peak may be observed directly at this plane, or the peak may be relayed (with magnification) to the detector (VersArray 1024BFT) for convenience. The relay lens used here is a 10× finite conjugate microscope objective with 0.25 NA (Newport M-10×). The relay NA must be much larger than the angle subtended by the virtual aperture to avoid additional diffraction of the peak. The relay NA should also be larger than the fiber NA to ensure that it does not vignette beam and reduce the intensity, but this effect is less critical. When a relay is used, alignment is similar, but a marker object (pinhead) can first be aligned at the position of the source as above, and the relay/detector system can then be aligned and focused on the reference object. If a square plate beam-splitter is used, it may be useful to rotate the plate in its plane to reduce the effect of multiple reflections on the background even when antireflection coatings are used.

Data are collected by taking two measurements of the peak for two different fiber positions. Small translations of the fiber on the order of hundreds of microns have negligible effect on the distribution of the diffusely scattered baseline, however, the peak shifts by exactly the same distance as the fiber. In this manner, two peaks are collected as shown in the left of Fig. 3. For all measurements, the background is measured with black cloth covering the sample and is

#139056 - $15.00 USD Received 20 Dec 2010; revised 28 Apr 2011; accepted 27 May 2011; published 6 Jun 2011

subtracted from the raw data to remove any light scattered from the beam-splitter. The right of the figure shows the ratio of these two background-subtracted peaks. Since the diffuse baseline component is the same in each peak, the result is a flat baseline and inverted peak. It should be noted that the baseline has a broad shape with maximum intensity near the center that can appear to be a peak with maximum value just to the lower right of the EBS peak in the upper left panel of Fig. 3, however this shape does not change with fiber position, and has no affect on the final measurement.

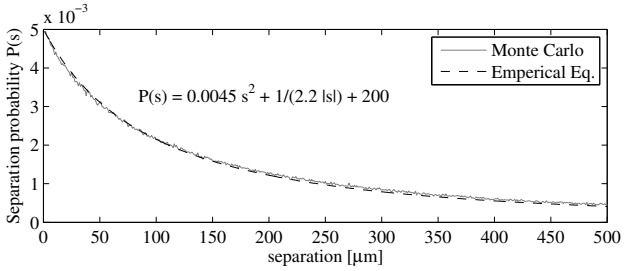

Fig. 4. Monte Carlo simulations were used to determine the probability $P(s)$ of path-pair separations for 0.2 μm diameter polystyrene beads suspended in water. The rays exiting the suspension were binned according to the exit radius from the entrance point and plotted above. The empirical equation shown was fit to the simulation and used in the numerical integration of Eq. (3).

To reduce noise, the peak is rotationally averaged out to some radius that falls between the positive and inverted peak. The peak shape can then be studied as a function of sample distance, material scattering properties, etc. Figure 5 shows the measured peak along with intensity values calculated by numerically integrating a two dimensional version of Eq. (3) for one entrance point at $x_1 = y_1 = 0$ and applying an experimentally determined factor of 0.43 to the peak to account for depolarization. The depolarization factor was obtained by taking the ratio of measured peaks with and without a linear polarizer sheet covering the sample. $P(s)$ was obtained from Monte Carlo simulation [15] and an equation shown in Fig. 4 was empirically fit to the simulated data. This Monte Carlo method uses random sampling of the probability distribution of scattering angle (sometimes called phase function), determined in this case by Mie theory. Rays are traced as they scatter in the medium and their exit locations are recorded to provide a numerical simulation of $P(s)$. We then fit a second order polynomial for use in the analytical equation. Although polarization effects are significant for this particle size, we treat polarization indirectly by rotationally averaging the exit locations to compute $P(s)$ and compare to unpolarized experimental results which include all polarization states. In this case, the primary effect of the medium dependent depolarization is to increase the incoherent baseline relative to the peak, and this is accounted for by the measured depolarization factor.

The coherence function was calculated assuming the fiber core was a uniform source with radius of 25 μm a distance z_0 away from the sample [16]. The numerical integration was performed out to a radius twice the illumination area which accounts for an increase in the baseline due to light that is returned without an associated path pair. By changing z_0, the spatial coherence length can be scanned, $L_{sc} = z_0/(k\rho)$ for source radius ρ. The inset shows the dependence of the peak on sample distance with enhancement increasing with L_{sc}. The scaling is due to the change in the spatial coherence function, $C(s)$, relative to $P(s)$.

As a demonstration of weak localization of light in three dimensions, the peak was measured over a range of detector positions for a fixed source–sample distance. The detector was scanned relative to the relay objective, and the corresponding object-space position relative to

#139056 - $15.00 USD Received 20 Dec 2010; revised 28 Apr 2011; accepted 27 May 2011; published 6 Jun 2011

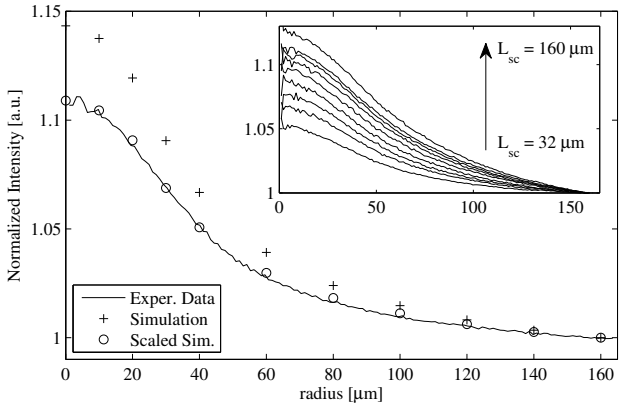

Fig. 5. Peak from 0.2 μm diameter microsphere suspension with transport mean free path $l_s' = 100$ μm. The baseline approaches one for all peaks, but small changes in intensity of the two measurements cause variation in the baseline values on the order of a few percent. The curves were therefore normalized to unity at a large radius for comparison. The simulated peak agrees well with the experimental data aside from a scaling factor of 0.76 which may be due to experimental error or simplifications in the theory (see conclusions). The inset shows the change in enhancement as a function of fiber–sample distance. As z_0 increases, L_{sc} increases and $C(s)$ broadens relative to $P(s)$ resulting in greater enhancement.

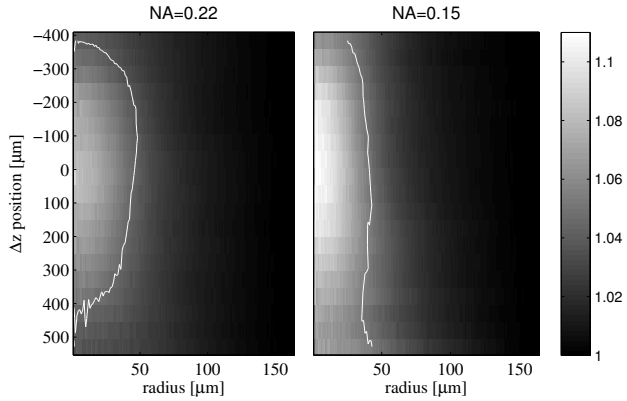

Fig. 6. Intensity through focus for a full spot size (left) and reduced spot size (right). The energy is weakly localized in three dimensions as expected. The smaller spot size results in a longer distribution along Δz analogous to an increase in depth of focus from a reduced NA. The line indicates the half-maximum contour.

the conjugate plane $\Delta z = z - z_0$ was calculated using the objective's longitudinal magnification and shown as Δz in Fig. 6.

The Δz-dependence of the peak is dominated by the effect of the illumination NA. As shown earlier, the lateral shape of the peak is the result of diffraction by the virtual aperture. For the geometry in the this experiment, the size of the virtual aperture extends a few hundred microns. However, the illumination spot is comprised of many such virtual apertures, each of which forms a peak convergent at the conjugate plane. The Δz-dependence of the peak is then analogous to depth of focus given the angular extent of the illuminated spot. This was confirmed by taking measurements of the peak through Δz for a full illumination spot and for

#139056 - $15.00 USD Received 20 Dec 2010; revised 28 Apr 2011; accepted 27 May 2011; published 6 Jun 2011

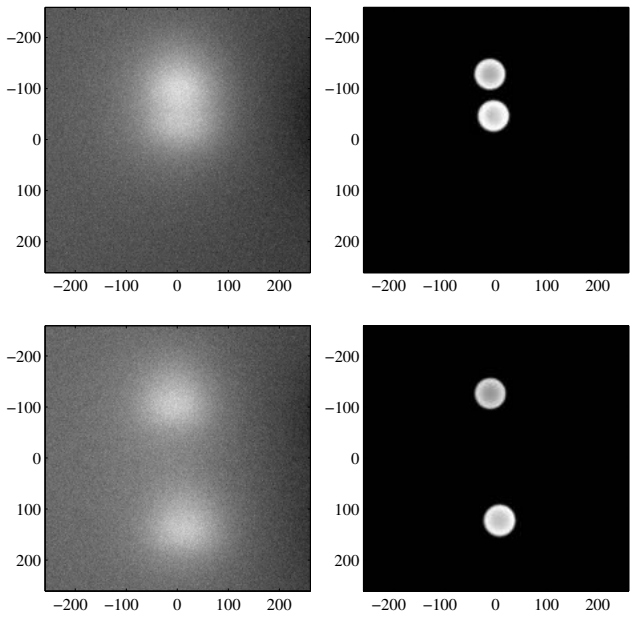

Fig. 7. Peak formed by a pair of fibers at two different separations. On the right, direct images of the fibers are shown. Scales are μm.

a reduced illumination spot where a black card with a small hole was placed over the sample to reduce the NA, shown on the right side of Fig. 6. To predict the depth of focus, the peak was approximated as Gaussian with 100 μm width and convolved with a $rect()$ of width y that results in half the maximum value at the center. The depth of focus is then $d_z \approx y/NA$. For the full NA 0.22 (left), d_z is estimated to be 900 μm and for the reduced NA of 0.15 (right), d_z is estimated to be 1300 μm, which agrees qualitatively with the result in Fig. 6 although noise limited measurements for Δz larger than the range shown.

As discussed before, the use of an extended incoherent source results in partial spatial coherence. This can be treated by multiplying the virtual aperture by the coherence function (which can be calculated by the van Cittert–Zernike theorem) or by superposition of the EBS peak with the source function. This superposition can be demonstrated by using a pair of fibers for illumination. Figure 7 shows EBS peaks formed by two different fiber pairs with different spacing. The right panels show images taken at the same magnification of the illuminating fibers themselves. This highlights a consequence of phase conjugation, that a random scattering medium can act as an imaging system producing an image of the source without any intervening optics. The image formed is a convolution of the object with the Point Spread Function (PSF) of the system, the effect of diffraction from the virtual aperture $P(s)$.

4. Conclusions

We have presented an alternate theoretical description and geometry for observation of weak localization of light and outlined a number of key physical concepts. The noteworthy physical concepts are: (1) the ensemble average intensity of light backscattered from a random medium can be described by an appropriate superposition of Huygens wavelets resulting in an incoherent diffuse baseline and an EBS peak; (2) the EBS peak is the result of phase conjugation of a portion of the incident wavefront; (3) the intensity peak can be represented as diffraction of a virtual aperture function $P(s)$ that describes the probability distribution of path-pair separa-

#139056 - $15.00 USD Received 20 Dec 2010; revised 28 Apr 2011; accepted 27 May 2011; published 6 Jun 2011

tions; (4) an extended source forms a superposition of EBS peaks from each point in the source and can be calculated in Fourier space by multiplying $P(s)$ with the coherence function $C(s)$.

There are some differences from the traditional configuration that may result in subtle effects that have not been investigated within the scope of this paper. First, the flat wavefront in a collimated configuration matches the shape of the surface, whereas the in our case a diverging spherical wavefront illuminates a flat surface. This mismatch is expected to cause subtle effects, i.e. amplitude falloff and an increase in the spatial coherence at the edge of the illumination compared to the center. This also leads to a degree of asymmetry in $P(s)$ due to local relative tilt between the wavefront and the sample surface at each location. Second, computational resources limited the integration of Eq. (3) plotted in Fig. 5 to a single entrance point at the center of the spot. Evaluating the integral for all entrance points including those closer to the edge of the spot may also reduce the peak enhancement. It is possible that these effects contribute to the scaling error between the predicted peak and the observed peak in Fig. 5 and further work will be needed to explore this.

The experimental configuration described in this paper has some practical advantages: (1) simpler alignment and implementation; (2) fewer components reduces background and stray light; (3) dependence of spatial coherence on the source-sample distance allows the scanning of spatial coherence. The simplicity of the configuration and potential for miniaturization make this geometry attractive for development as a portable instrument and for *in vivo* measurements for biomedical applications like tissue characterization [15]. Phase conjugation also implies that aberrations or phase errors introduced between the beam-splitter and the medium will not degrade the peak shape. The theoretical description summarized by Eq. (3) offers a way to numerically calculate values of backscattered intensity from a material described by $P(s)$ that can take into account realistic experimental parameters such as finite spot size. Finally, we demonstrate the obvious but interesting consequence that a random medium can form an image of any source without the use of lenses.

Acknowledgments

This research was supported by the National Institutes of Health grants R01CA128641 and R01EB003682.

#139056 - $15.00 USD Received 20 Dec 2010; revised 28 Apr 2011; accepted 27 May 2011; published 6 Jun 2011